

Origin of Jahn-Teller Distortion and Orbital Order in LaMnO_3

Eva Pavarini and Erik Koch

Institut für Festkörperforschung and Institute for Advanced Simulation, Forschungszentrum Jülich, 52425 Jülich, Germany
(Received 30 April 2009; published 22 February 2010)

The origin of the cooperative Jahn-Teller distortion and orbital order in LaMnO_3 is central to the physics of the manganites. The question is complicated by the simultaneous presence of tetragonal and GdFeO_3 -type distortions and the strong Hund's rule coupling between e_g and t_{2g} electrons. To clarify the situation we calculate the transition temperature for the Kugel-Khomskii superexchange mechanism by using the local density approximation + dynamical mean-field method, and disentangle the effects of superexchange from those of lattice distortions. We find that superexchange alone would yield $T_{\text{KK}} \sim 650$ K. The tetragonal and GdFeO_3 -type distortions, however, reduce T_{KK} to ~ 550 K. Thus electron-phonon coupling is essential to explain the persistence of local Jahn-Teller distortions to ≥ 1150 K and to reproduce the occupied orbital deduced from neutron scattering.

DOI: 10.1103/PhysRevLett.104.086402

PACS numbers: 71.10.Fd, 71.10.Hf, 71.27.+a

The insulating perovskite LaMnO_3 is the parent compound of the colossal magnetoresistance manganites [1] and it is considered a textbook example of a cooperative Jahn-Teller (JT) orbitally ordered material [2]. Two distinct mechanisms have been proposed to explain the cooperative distortion: many-body Kugel-Khomskii (KK) superexchange (SE) [3] and one-electron electron-phonon (EP) coupling [4]. Determining the relative strength of these mechanisms will provide a measure of the importance of strong correlation effects for the orbital physics in the manganites. Unfortunately, the situation is complicated by the simultaneous presence of tetragonal and GdFeO_3 -type distortions as well as a strong Hund's rule coupling between the Mn e_g and t_{2g} electrons.

In LaMnO_3 the Mn^{3+} ions are in a $t_{2g}^3 e_g^1$ configuration. Because of strong Hund's rule coupling the spin of the e_g electron is parallel to the spin of the t_{2g} electrons on the same site. Above $T_N = 140$ K the spins on neighboring sites are disordered [5]. The crystal structure is orthorhombic (Fig. 1). It can be understood by starting from an ideal cubic perovskite structure with axes \mathbf{x} , \mathbf{y} , and \mathbf{z} : first, a tetragonal distortion reduces the Mn-O bond along \mathbf{z} by 2%. The La-O and La-Mn covalencies induce a GdFeO_3 -type distortion [6,7] resulting in an orthorhombic lattice with axes \mathbf{a} , \mathbf{b} , and \mathbf{c} , with the oxygen-octahedra tilted about \mathbf{b} and rotated around \mathbf{c} in alternating directions. Finally, the octahedra distort, with long (l) and short (s) bonds alternating along \mathbf{x} and \mathbf{y} , and repeating along \mathbf{z} [8–11]. This is measured by $\delta_{\text{JT}} = (l - s)/((l + s)/2)$. The degeneracy of the e_g orbitals is lifted and the occupied orbital, $|\theta\rangle = \cos\frac{\theta}{2}|3z^2 - 1\rangle + \sin\frac{\theta}{2}|x^2 - y^2\rangle$, is $\sim |3l^2 - 1\rangle$, i.e., it points in the direction of the long axis. Thus orbital order (OO) is d -type with the sign of θ alternating along \mathbf{x} and \mathbf{y} and repeating along \mathbf{z} . At 300 K the JT distortion is substantial, $\delta_{\text{JT}} = 11\%$, and $\theta \sim 108^\circ$ was estimated from neutron scattering data [8]. Above $T_{\text{OO}} \sim 750$ K a strong reduction to $\delta_{\text{JT}} = 2.4\%$ was reported [8,12], accompanied

by a change in θ to $\sim 90^\circ$ [8]. Recently this was, however, identified as an order-to-disorder transition [10,11]: because of orientational disorder, the crystal appears cubic on average, while, within nanoclusters, the MnO_6 octahedra remain fully JT distorted up to $T_{\text{JT}} \geq 1150$ K [11].

Model calculations based on superexchange alone can account for d -type order, but yield, for the classical ground state, $\theta \sim 90^\circ$ [13]. Models of electron-phonon coupling in simple cubic perovskites instead give $\sim 120^\circ$ [4]. To explain the observed $\sim 108^\circ$, one might thus conclude that both mechanisms are of similar importance [3]. Such models are lacking, however, a realistic description of the crystal and the calculated θ is sensitive to the choice of parameters [4,14]. LDA + U calculations yield $\theta = 109^\circ$

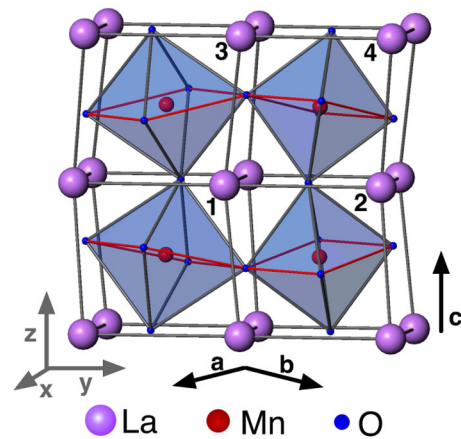


FIG. 1 (color online). Structure of LaMnO_3 at 300 K [8]. The conventional cell is orthorhombic with axes \mathbf{a} , \mathbf{b} , and \mathbf{c} , and contains 4 formula units. The pseudocubic axes (left corner) are defined via $\mathbf{a} = (\mathbf{x} - \mathbf{y})(1 + \alpha)$, $\mathbf{b} = (\mathbf{x} + \mathbf{y})(1 + \beta)$, and $\mathbf{c} = 2\mathbf{z}(1 + \gamma)$, with α , β , γ small numbers. For sites 1 and 3 the long (short) bond l (s) is \sim along \mathbf{y} (\mathbf{x}), vice versa for sites 2 and 4 (d -type pattern). All Mn sites are equivalent. The symmetries that transform them into a site of type 1 are $x \leftrightarrow y$ (site 2) $z \rightarrow -z$ (site 3), $x \leftrightarrow y$, $z \rightarrow -z$ (site 4).

and show that Coulomb repulsion is fundamental to stabilize the Jahn-Teller distortions in the ground state [15]. This might be taken as evidence that Kugel-Khomskii superexchange is the dominant mechanism, and electron-phonon coupling, enhanced by electron localization [15,16], merely helps. On the other hand, recent semiclassical many-body calculations for model cubic perovskites indicate that electron-phonon coupling is essential to explain orbital ordering above 300 K [17].

While it is not obvious how well LDA + U or semiclassical approaches capture the many-body nature of the KK superexchange, it seems clear that the inclusion of the real crystal structure is crucial [3,6,18,19]. The tetragonal and GdFeO₃-type distortions result in a sizable narrowing of the e_g bands [6,7,20], likely changing the relative strength of superexchange and electron-phonon coupling. Since, in the presence of a crystal field, Coulomb repulsion suppresses orbital fluctuations [6,21], they may even compete with SE and EP coupling. To identify the driving mechanism for orbital order in LaMnO₃, it is thus mandatory to account for both the realistic electronic structure and many-body effects. To understand the mechanism one has to disentangle the contribution of KK superexchange from that of the JT or the GdFeO₃-type and tetragonal distortions.

In this Letter, we do this by calculating directly the Kugel-Khomskii superexchange transition temperature T_{KK} with and without tetragonal and GdFeO₃-type distortions. We adopt the method used successfully for KCuF₃ [21], based on local-density approximation (LDA) + dynamical mean-field theory (DMFT) [22].

First, we calculate the electronic structure *ab initio* using the N th order muffin-tin orbital method. Since the Hund's rule energy gain is larger than the e_g - t_{2g} crystal-field splitting, the t_{2g} bands are $\frac{1}{2}$ filled and the e_g bands $\frac{1}{4}$ filled; the three t_{2g} electrons behave as a spin $\mathbf{S}_{t_{2g}}$ and couple to the e_g electron via an effective magnetic field $h = JS_{t_{2g}}$. In the paramagnetic phase ($T > T_N = 140$ K) the t_{2g} spins are spatially disordered. The minimal model to study the KK mechanism in LaMnO₃ is thus [23]

$$H = \sum_{im\sigma, jm'\sigma'} t_{m,m'}^{i,i'} u_{\sigma,\sigma'}^{i,i'} c_{im\sigma}^\dagger c_{j'm'\sigma'} - h \sum_{im} (n_{im\uparrow} - n_{im\downarrow}) + U \sum_{im} n_{im\uparrow} n_{im\downarrow} + \frac{1}{2} \sum_{im(\neq m')\sigma\sigma'} (U - 2J - J\delta_{\sigma,\sigma'}) n_{im\sigma} n_{im'\sigma'}. \quad (1)$$

$c_{im\sigma}^\dagger$ creates an electron with spin $\sigma = \uparrow, \downarrow$ in a Wannier orbital $|m\rangle = |x^2 - y^2\rangle$ or $|3z^2 - 1\rangle$ at site i , and $n_{im\sigma} = c_{im\sigma}^\dagger c_{im\sigma}$. \uparrow (\downarrow) indicates the e_g spin parallel (antiparallel) to the t_{2g} spins (on that site). The matrix u ($u_{\sigma,\sigma'}^{i,i'} = 2/3$ for $i \neq i'$, $u_{\sigma,\sigma'}^{i,i} = \delta_{\sigma,\sigma'}$) accounts for the orientational disorder of the t_{2g} spins [23]; $t_{m,m'}^{i,i'}$ is the LDA hopping integral

from orbital m on site i to orbital m' on site i' , obtained *ab initio* by downfolding the LDA bands and constructing a localized e_g Wannier basis. The on-site terms $i = i'$ give the crystal-field splitting. U and J are the direct and exchange screened on-site Coulomb interaction [24]. We use the theoretical estimate $J = 0.75$ eV [25] and vary U between 4 and 7 eV. The Hund's rule splitting was estimated *ab initio* to $2JS_{t_{2g}} \sim 2.7$ eV [7]. We solve (1) using DMFT [26] or cellular DMFT (CDMFT) and a quantum Monte Carlo [27] solver, working with the full self-energy matrix $\Sigma_{mm'}$ in orbital space [6]. The spectral matrix on the real axis is obtained by analytic continuation [28].

We consider several structures: (i) the room temperature structure R_{11} with $\delta_{\text{JT}} = 11\%$, and a series of hypothetical structures $R_{\delta_{\text{JT}}}$ with reduced JT distortion δ_{JT} , (ii) the (average) structure found at 800 K, $R_{2.4}^{800\text{K}}$, which has a slightly larger volume than R_{11} and a smaller GdFeO₃-type distortion, and (iii) the ideal cubic structure I_0 with the same volume as R_{11} . For all structures we find that at each site the e_g spins align to $\mathbf{S}_{t_{2g}}$. We calculate the orbital polarization p as a function of temperature [29] by diagonalizing the DMFT (or CDMFT) occupation matrix and taking the difference between the occupation of the most ($|\theta\rangle$) and least ($|\theta + \pi\rangle$) filled orbital. To test the t_{2g} spins picture we perform calculations for the 5-band ($e_g + t_{2g}$) Hubbard model [30]. We find that it holds even at high temperatures.

For the 300 K structure (R_{11}) the bandwidths are $W_{t_{2g}} \sim 1.6$ eV and $W_{e_g} \sim 3.0$ eV. The e_g states split by ~ 840 meV, in good agreement with experimental estimates [31]. The lower crystal-field state at site 1 is $|1\rangle = 0.574|3z^2 - 1\rangle + 0.818|x^2 - y^2\rangle$. We find an insulating solution in the full range $U = 4$ –7 eV (Fig. 2). The Mott gap E_g is ~ 0.6 eV for $U = 4$ eV, and increases almost linearly with increasing U . For $U = 5$ eV, suggested by recent estimates [7,32], the Hubbard bands are at ~ -1.5 and 2 eV. In addition there is a broad feature around 5 eV due to e_g states with spin antiparallel to the randomly oriented t_{2g} spins. These spectra are in line with experiments [31–34]. We find that even at 1150 K the system is fully orbitally polarized ($p \sim 1$). On sites 1 and 3, the

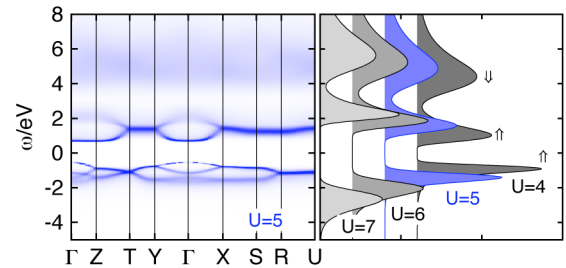


FIG. 2 (color online). Right: LDA + DMFT spectral function for the room temperature structure R_{11} for different U . \uparrow (\downarrow) indicates states with e_g spins parallel (antiparallel) to $\mathbf{S}_{t_{2g}}$. Left: \mathbf{k} -resolved spectral function for $U = 5$ eV.

occupied state is $|\theta\rangle \sim |106^\circ\rangle$, on sites 2 and 4 it is $|\theta\rangle \sim |-106^\circ\rangle$ (d -type OO); $|\theta\rangle$ is close to the lower crystal-field state obtained from LDA (Table I) and in excellent agreement with neutron diffraction experiments [8]. We find that things hardly change when the JT distortion is halved (R_6 structure in Fig. 3). Even for the average 800 K structure ($R_{2.4}^{800\text{ K}}$) OO does not disappear: Although the Jahn-Teller distortion is strongly reduced to $\delta_{\text{JT}} = 2.4\%$, the crystal-field splitting is ~ 168 meV and the orbital polarization at 1150 K is as large as $p \sim 0.65$, while θ is now close to 90° . For all these structures, orbital order is already determined by the distortions via the crystal-field splitting.

To find the temperature T_{KK} at which Kugel-Khomskii superexchange drives orbital order we consider the zero crystal-field limit, i.e., the ideal cubic structure I_0 . The e_g bandwidth increases to $W_{e_g} \sim 3.7$ eV and for $U = 5$ eV the system is a Mott insulator with a tiny gap only below $T \sim 650$ K. We find $T_{\text{KK}} \sim 650$ K, very close to the metal-insulator transition (Fig. 3). To check how strongly T_{KK} changes when the gap opens, we increase U . For $U = 5.5$ eV we find an insulating solution with a small gap of ~ 0.5 eV and T_{KK} still close to ~ 650 K. For $U = 6$ eV, $E_g \sim 0.9$ eV and $T_{\text{KK}} \sim 550$ K. Even with an unrealistically large $U = 7$ eV, giving $E_g \sim 1.8$ eV, T_{KK} is still as large as ~ 470 K. Thus, despite the small gap, T_{KK} decreases as $\sim 1/U$, as expected for superexchange. For a realistic $U \sim 5$ eV, the calculated $T_{\text{KK}} \sim 650$ K is surprisingly close to the order-disorder transition temperature, $T_{\text{OO}} \sim 750$ K, though still much smaller than $T_{\text{JT}} \geq 1150$ K. The occupied state at site 1 is $|\theta\rangle \sim |90^\circ\rangle$ for all U .

Such a large T_{KK} is all the more surprising when compared with the value obtained for KCuF_3 , $T_{\text{KK}} \sim 350$ K [21]. For the ideal cubic structure the hopping matrix (Table I) is $t_{m,m'}^{i,i\pm z} \sim -t\delta_{m,m'}\delta_{m,3z^2-1}$, $t_{m,m'}^{i,i\pm x} = t_{m,m'}^{i,i\pm y} \sim -t/4(1 + 2\delta_{m,x^2-y^2})$, and for $m \neq m'$ $t_{m,m'}^{i,i\pm x} = -t_{m,m'}^{i,i\pm y} \sim \sqrt{3}t/4$. Since the effective (after averaging over the direc-

tions of $\mathbf{S}_{t_{2g}}$) hopping integral in LaMnO_3 , $2t/3 \sim 345$ meV is $\sim 10\%$ smaller than $t \sim 376$ meV in KCuF_3 [21], one may expect a slightly smaller T_{KK} in LaMnO_3 , opposite to what we find. Our result can, however, be understood in superexchange theory. The KK SE part of the Hamiltonian, obtained by second-order perturbation theory in t from Eq. (1), may be written as

$$H_{\text{SE}}^{i,i'} \sim \frac{J_{\text{SE}}}{2} \sum_{\langle i,i' \rangle_{\mathbf{x},\mathbf{y}}} [3T_i^x T_{i'}^x \mp \sqrt{3}(T_i^z T_{i'}^x + T_i^x T_{i'}^z)] + \frac{J_{\text{SE}}}{2} \sum_{\langle i,i' \rangle_{\mathbf{x},\mathbf{y}}} T_i^z T_{i'}^z + 2J_{\text{SE}} \sum_{\langle i,i' \rangle_{\mathbf{z}}} T_i^z T_{i'}^z, \quad (2)$$

where $\langle i, i' \rangle_{\mathbf{x},\mathbf{y}}$ and $\langle i, i' \rangle_{\mathbf{z}}$ indicate near neighboring sites along \mathbf{x} , \mathbf{y} , or \mathbf{z} ; $-(+)$ refers to the \mathbf{x} (\mathbf{y}) direction, T_i^x and T_i^z are pseudospin operators [3], with $T^z|3z^2-1\rangle = 1/2|3z^2-1\rangle$, $T^z|x^2-y^2\rangle = -1/2|x^2-y^2\rangle$. The superexchange coupling is $J_{\text{SE}} = (\bar{t}^2/U)(w/2)$, where \bar{t} is the effective hopping integral. In the large U limit (negligible J/U and h/U), $w \sim 1 + 4\langle S_i^z \rangle \langle S_{i'}^z \rangle + (1 - 4\langle S_i^z \rangle \langle S_{i'}^z \rangle) \langle S_i^z \rangle u_{\uparrow,\downarrow}^{i,i'}/u_{\uparrow,\uparrow}^{i,i'}$, where S_i^z are the e_g spin operators. In LaMnO_3 the e_g spins align with the randomly oriented t_{2g} spins, thus $\bar{t} = 2t/3$, $w \sim 2$, and $J_{\text{SE}} \sim 2(2t/3)^2/U$. For d -type order, the classical ground state is $|\theta\rangle \sim |90^\circ\rangle$, in agreement with our DMFT results. In KCuF_3 , with configuration $t_{2g}^6 e_g^3$, the Hund's rule coupling between e_g and t_{2g} plays no role, i.e., $\langle S_i^z \rangle = 0$. The hopping integral $\bar{t} = t$ is indeed slightly larger than in LaMnO_3 , but $w \sim 1$, a reduction of 50%. Consequently, J_{SE} is reduced by ~ 0.6 in KCuF_3 . For finite J/U and h/U , w is a more complicated function, but the conclusions stay the same. We verified solving (1) with LDA + DMFT that also for LaMnO_3 T_{KK} drops drastically if $u_{\sigma,-\sigma}^{i,i'} = 0$ and $h = 0$.

TABLE I. Hopping integrals $t_{m,m'}^{i,i'}$ /meV from a site i of type 1 to a neighboring site i' of type 2 in direction $l\mathbf{x} + n\mathbf{y} + m\mathbf{z}$ for structures R_{11} , $R_{2.4}^{800\text{ K}}$, R_0 , and I_0 . The states m, m' are $|\pi\rangle = |x^2 - y^2\rangle$ and $|0\rangle = |3z^2 - 1\rangle$. The crystal-field states are the eigenvectors of the on-site matrix ($l = m = n = 0$).

lmn	$t_{\pi,\pi}^{i,i'}$	$t_{\pi,0}^{i,i'}$	$t_{0,\pi}^{i,i'}$	$t_{0,0}^{i,i'}$	$t_{\pi,\pi}^{i,i'}$	$t_{\pi,0}^{i,i'}$	$t_{0,\pi}^{i,i'}$	$t_{0,0}^{i,i'}$
	R_{11}				$R_{2.4}^{800\text{ K}}$			
000	0	409	409	305	0	84	84	-2
001	-8	-47	-47	-445	-2	-13	-13	-439
010	-322	233	174	-129	-328	196	190	-105
100	-322	-174	-236	-129	-328	-190	-196	-105
	R_0				I_0			
000	0	5	5	218	0	0	0	0
001	-1	-2	-2	-433	-10	0	0	-518
010	-333	206	207	-121	-391	220	220	-137
100	-333	-207	-206	-121	-391	-220	-220	-137

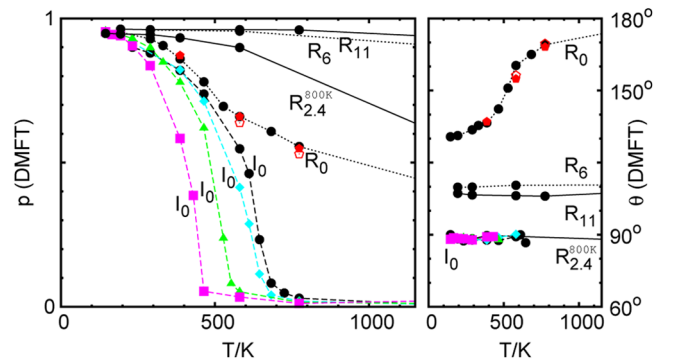


FIG. 3 (color online). Orbital polarization p (left) and (right) occupied state $|\theta\rangle$ ($|\theta\rangle$) for sites 1 and 3 (2 and 4) as a function of temperature. Solid line: 300 K (R_{11}) and 800 K ($R_{2.4}^{800\text{ K}}$) structures. Dots: orthorhombic structures with half (R_6) or no (R_0) Jahn-Teller distortion. Pentagons: 2 (full) and 4 (empty) sites CDMFT. Dashes: ideal cubic structure (I_0). Circles: $U = 5$ eV. Diamonds: $U = 5.5$ eV. Triangles: $U = 6$ eV. Squares: $U = 7$ eV. Crystal-field splitting (meV): 840 (R_{11}), 495 (R_6), 219 (R_0), 168 ($R_{2.4}^{800\text{ K}}$), and 0 (I_0).

It remains to evaluate the effect of the orthorhombic distortion on the transition. For this we perform calculations for the system R_0 with no Jahn-Teller distortion, but keeping the tetragonal and GdFeO_3 -type distortion of the 300 K structure. This structure is metallic for $U = 4$ eV; for $U = 5$ eV it has a gap of ~ 0.5 eV. We find a large polarization already at 1150 K ($p \sim 0.45$). Such polarization is due to the crystal-field splitting of about 219 meV, with lower crystal-field states at site 1 given by $|1\rangle \sim |x^2 - y^2\rangle$. Surprisingly, the most occupied state $|\theta\rangle$ is close to $|1\rangle$ ($\theta \sim 180$) only at high temperature (~ 1000 K). The orthorhombic crystal field thus competes with superexchange, analogous to an external field with a component perpendicular to an easy axis. On cooling the occupied orbitals rotate to $|\theta\rangle \sim |132^\circ\rangle$ (see Fig. 3). This effect of superexchange occurs around a characteristic temperature $T_{\text{KK}}^R \sim 550$ K, still surprisingly large, but reduced compared to T_{KK} for the ideal cubic system I_0 and much smaller than the experimental $T_{\text{JT}} \geq 1150$ K. Short-range correlations could reduce T_{KK}^R or modify θ . To estimate this effect we perform CDMFT calculations; our results (Fig. 3) remain basically unchanged. Thus, electron-phonon coupling is necessary to explain both the transition temperature and the correct occupied orbital $|\theta\rangle \sim |108^\circ\rangle$.

In conclusion, we find that T_{KK}^R in orthorhombic LaMnO_3 is ~ 550 K. We have shown that two elements are crucial: the superexchange mechanism, which yields a transition temperature as high as 650 K, and the tetragonal plus GdFeO_3 -type distortion, which, due to the reduced hopping integrals and the competing orthorhombic crystal field, reduces T_{KK} to 550 K. Experimentally, an order-to-disorder transition occurs around $T_{\text{OO}} \sim 750$ K, but a local Jahn-Teller distortion persists in the disordered phase up to $T_{\text{JT}} \geq 1150$ K. The Kugel-Khomskii mechanism alone cannot account for the presence of such Jahn-Teller distortions above 550 K ($T_{\text{KK}}^R \ll T_{\text{JT}}$). It also cannot justify the neutron scattering estimate $\theta = 108^\circ$. Thus electron-phonon coupling is a crucial ingredient, both for making the Jahn-Teller distortions energetically favorable at such high temperatures and in determining the occupied orbital.

We acknowledge discussions with D. I. Khomskii and A. I. Lichtenstein, and Grant No. JIFF22 on Jugene.

[1] Y. Tokura and N. Nagaosa, *Science* **288**, 462 (2000).
 [2] P. Fazekas, *Lecture Notes on Electron Correlation and Magnetism* (World Scientific, Singapore, 1999).
 [3] K. I. Kugel and D. I. Khomskii, *Zh. Eksp. Teor. Fiz.* **64**, 1429 (1973) [*Sov. Phys. JETP* **37**, 725 (1973)].
 [4] J. Kanamori, *J. Appl. Phys.* **31**, S14 (1960).
 [5] E. O. Wollan and W. C. Koehler, *Phys. Rev.* **100**, 545 (1955).
 [6] E. Pavarini *et al.*, *Phys. Rev. Lett.* **92**, 176403 (2004); M. De Raychaudhury, E. Pavarini, and O. K. Andersen, *ibid.*

99, 126402 (2007); E. Pavarini, A. Yamasaki, J. Nuss, and O. K. Andersen, *New J. Phys.* **7**, 188 (2005).
 [7] A. Yamasaki *et al.*, *Phys. Rev. Lett.* **96**, 166401 (2006).
 [8] J. Rodríguez-Carvajal *et al.*, *Phys. Rev. B* **57**, R3189 (1998).
 [9] T. Chatterji *et al.*, *Phys. Rev. B* **68**, 052406 (2003).
 [10] M. C. Sánchez, G. Subías, J. García, and J. Blasco, *Phys. Rev. Lett.* **90**, 045503 (2003).
 [11] X. Qiu, Th. Proffen, J. F. Mitchell, and S. J. L. Billinge, *Phys. Rev. Lett.* **94**, 177203 (2005); A. Sartbaeva *et al.*, *ibid.* **99**, 155503 (2007).
 [12] Y. Murakami *et al.*, *Phys. Rev. Lett.* **81**, 582 (1998).
 [13] J. Bala and A. M. Oleś, *Phys. Rev. B* **62**, R6085 (2000).
 [14] R. Maezono, S. Ishihara, and N. Nagaosa, *Phys. Rev. B* **58**, 11583 (1998).
 [15] W. G. Yin, D. Volja, and W. Ku, *Phys. Rev. Lett.* **96**, 116405 (2006).
 [16] E. Koch and E. Pavarini (to be published).
 [17] C. Lin and A. J. Millis, *Phys. Rev. B* **78**, 174419 (2008).
 [18] T. Hotta, S. Yunoki, M. Mayr, and E. Dagotto, *Phys. Rev. B* **60**, R15009 (1999).
 [19] L. E. Gonchar' and A. E. Nikiforov, *Fiz. Tverd. Tela* **42**, 1038 (2000) [*Phys. Solid State* **42**, 1070 (2000)].
 [20] C. Ederer, C. Lin, and A. J. Millis, *Phys. Rev. B* **76**, 155105 (2007).
 [21] E. Pavarini, E. Koch, and A. I. Lichtenstein, *Phys. Rev. Lett.* **101**, 266405 (2008).
 [22] V. I. Anisimov *et al.*, *J. Phys. Condens. Matter* **9**, 7359 (1997); A. I. Lichtenstein and M. I. Katsnelson, *Phys. Rev. B* **57**, 6884 (1998).
 [23] K. H. Ahn and A. J. Millis, *Phys. Rev. B* **61**, 13545 (2000).
 [24] J. Kanamori, *Prog. Theor. Phys.* **30**, 275 (1963).
 [25] T. Mizokawa and A. Fujimori, *Phys. Rev. B* **54**, 5368 (1996).
 [26] A. Georges, G. Kotliar, W. Kraut, and M. J. Rozenberg, *Rev. Mod. Phys.* **68**, 13 (1996).
 [27] J. E. Hirsch and R. M. Fye, *Phys. Rev. Lett.* **56**, 2521 (1986).
 [28] J. E. Gubernatis, M. Jarrell, R. N. Silver, and D. S. Sivia, *Phys. Rev. B* **44**, 6011 (1991).
 [29] With e_g spins aligned to the t_{2g} spins, the SE coupling [see discussion after Eq. (2)] is $J_{\text{SE}} \sim 2t^2(1/(U-3J) + (u_{\uparrow,\downarrow}/u_{\uparrow,\uparrow}))(1/(U+2h-2J) - 1/(U+2h))$, i.e., depends weakly on the $u_{\sigma-\sigma}^{i'l}$ terms in (1); thus we neglect them.
 [30] Structure R_{11} , parameters $1/k_B T = 5$ eV, $U = 5$ eV, $J = 0.75$ eV. We find $\sim t_{2g}^3 e_g^1$ and Hubbard bands in line with $S_{t_{2g}} = 3/2$; the e_g orbital polarization, p and the gap are close to the results for Hamiltonian (1).
 [31] N. N. Kovaleva *et al.*, *Phys. Rev. Lett.* **93**, 147204 (2004).
 [32] J.-H. Park *et al.*, *Phys. Rev. Lett.* **76**, 4215 (1996).
 [33] K. Takenaka *et al.*, *J. Phys. Soc. Jpn.* **68**, 1828 (1999); J. H. Jung *et al.*, *Phys. Rev. B* **57**, R11043 (1998); M. A. Quijada *et al.*, *ibid.* **64**, 224426 (2001); K. Tobe *et al.*, *ibid.* **64**, 184421 (2001).
 [34] A. Chainani, M. Mathew, and D. D. Sarma, *Phys. Rev. B* **47**, 15397 (1993); T. Saitoh *et al.*, *ibid.* **51**, 13942 (1995); T. Saitoh *et al.*, *ibid.* **56**, 8836 (1997).